Magnetic Properties of Mechanically Milled Sm-Co Permanent Magnetic Materials with the TbCu$_7$ Structure

5.1. Introduction

Sm-Co permanent magnetic materials have the advantage of possessing higher Curie temperature than that of Nd-Fe-B permanent magnetic materials [1]. They exhibit three structural forms of CaCu$_5$, Th$_2$Zn$_{17}$ and Th$_2$Ni$_{17}$ [2,3]. In addition, the TbCu$_7$ structure is also observed, which is a disordered form of CaCu$_5$ structure having *P6/mmm* space group where one of the Sm atoms is replaced with a transition metal dumbbell pair randomly. The substitution for rare earth atoms by dumbbell pairs in an ordered fashion results in Th$_2$Zn$_{17}$ rhombohedral structure of the type $R\bar{3}m$. The substitution of Fe in Sm-Co system increases the magnetization whereas the addition of Zr or Cu helps in the stabilization of the TbCu$_7$ structure and also increases the anisotropy [4,5].

The Sm-Co permanent magnetic materials can be synthesized through mechanical alloying or melt spinning technique [6,7]. However, the synthesis through both the techniques results in the formation of two or more phases [8-10], which could affect the magnetic properties. A high coercivity of 688 kA/m at a temperature of 773 K has been achieved through proper heat treatments and development of cellular microstructure having Sm$_2$Co$_{17}$ as the main phase and SmCo$_5$ as the grain boundary phase [11]. The coercivity is found to decrease on grain size reduction for the TbCu$_7$ structure of Sm$_2$Co$_{17}$ particles separated by Cu particles, which is obtained by milling the annealed Sm-Co powder along with Cu as reported by Zhang *et al.* [12]. An enhancement in the coercivity and squareness ratio for lower milling durations of 15 min followed by a gradual deterioration due to amorphisation, on further milling, has been observed in the case of SmCo$_5$ permanent magnetic materials [3,13]. Ball milling SmCo$_5$ with antiferromagnetic powders such as NiO and CoO in an appropriate ratio has resulted in an enhanced coercivity and squareness ratio due to the coupling between both the phases [14,15]. The increase in coercivity is attributed to various reasons like grain size reduction and pinning of the domain walls by the phases

such as $SmCo_5$ and FeZrCu [16] that segregate at the grain boundary. In this chapter, the changes in the magnetic properties of the mechanically milled $Sm(Co,Fe,Cu,Zr)_7$ permanent magnetic material having the $TbCu_7$ structure are presented.

5.2.   Experiment

Elements of high purity Sm, Co, Fe, Cu and Zr were induction-melted in the weight percentage of 26, 51, 15, 5 and 3 respectively to form an ingot. The resulting ingot was hand-crushed for 5 minutes in an agate mortar in toluene medium to avoid oxidation. The ball milling was carried out using a high energy ball mill (Fritsch Pulveresette 7) with agate balls and vial in high purity toluene medium. The ball to powder weight ratio was fixed as 20:1 and the milling speed was 300 rpm. The X-ray diffraction (XRD) measurements were performed using Cu-K$_\alpha$ radiation. The average grain size was estimated using the Scherrer formula. Scanning electron microscopy (SEM) measurements were performed to study the morphology of the samples. Magnetic measurements at 300 K were carried out using a vibrating sample magnetometer (VSM) with a maximum applied field of 2 T by fixing the samples in wax in a cylindrical sample holder. Equal weight of sample was taken for all the measurements. Thermomagnetization (TM) measurements were performed in Ar atmosphere using a Perkin Elmer thermogravimetric analyzer (TGA) and a small horse shoe magnet with a field strength of 4 mT. [57]Fe Mössbauer experiments were carried out at 300 K using a Wiessel constant acceleration Mössbauer spectrometer with a Co-57/Rh source kept at 300 K. The spectrometer was calibrated with a natural iron foil before and after the experiments.

5.3.   Results and Discussion

5.3.1. Structure, grain size and morphology

Figure 5.1 shows the XRD patterns of the $Sm(Co,Fe,Cu,Zr)_7$ compound for various milling durations. The XRD patterns are indexed corresponding to the hexagonal *P6/mmm* phase with the $TbCu_7$ structure. The absence of the (015) peak of the Th_2Zn_{17} structure between (110) and (200) reflections suggests that the Th_2Zn_{17} structure is not present in the samples. The lattice parameters calculated from the XRD peak positions are   a = 4.903 Å
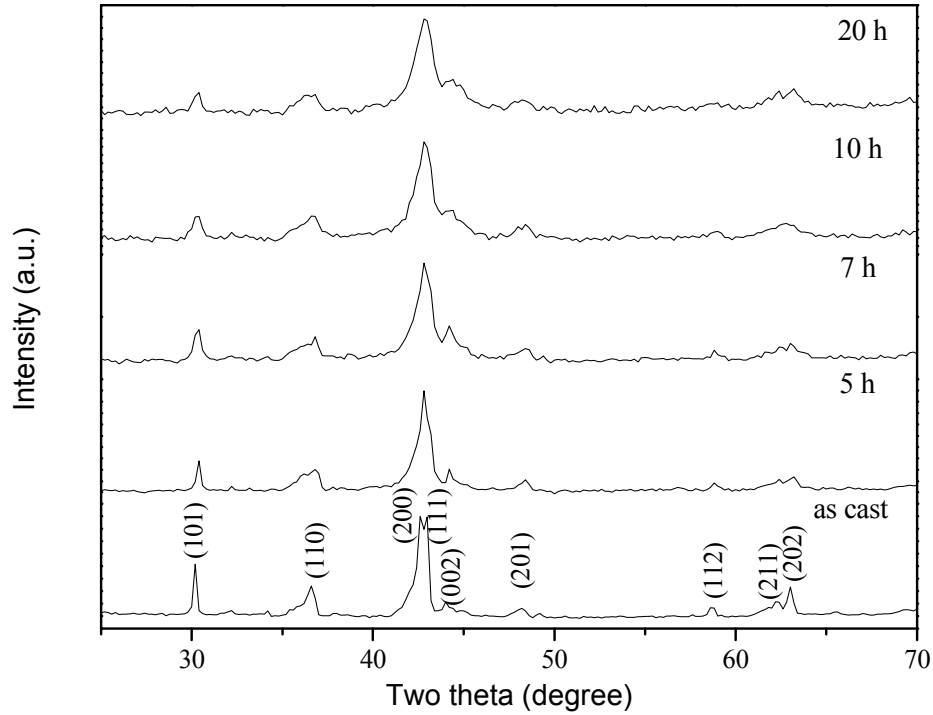
Fig. 5.1. The XRD of the Sm(Co,Fe,Cu,Zr)$_7$ compound with the TbCu$_7$ structure milled for various durations.

and c = 4.109 Å. The c/a ratio is 0.84 which is in agreement with the reported value for the TbCu$_7$ hexagonal structure [17] with a unit cell volume of 85.54 Å^3. The grain size decreases on milling as is evident from the broadening of the XRD peaks. The shoulder near the (110) peak occurs probably due to the disordered nature of TbCu$_7$ phase [18]. On milling, the (200) and (111) peaks merge into a single peak. The average grain size calculated, using the Scherrer formula, from the width of the (101) peak is found to decrease from 72 nm for the bulk to 15 nm for the 20 h milled sample as shown in Fig. 5.2.(a). However, there is no significant reduction in grain size when the milling duration is increased from 10 to 20 h.

The ball milling induces strain in the milled samples. The root mean square (r.m.s.) atomic level strain can be calculated using the relation [19]

$$< e^2 >^{1/2} = \frac{\beta_e}{2\eta \tan \theta}$$

where β_e is the full-width at the half-maximum of the (101) X-ray peak, η is the coefficient which depends on the distribution of strains and it is chosen as unity [19] assuming uniform
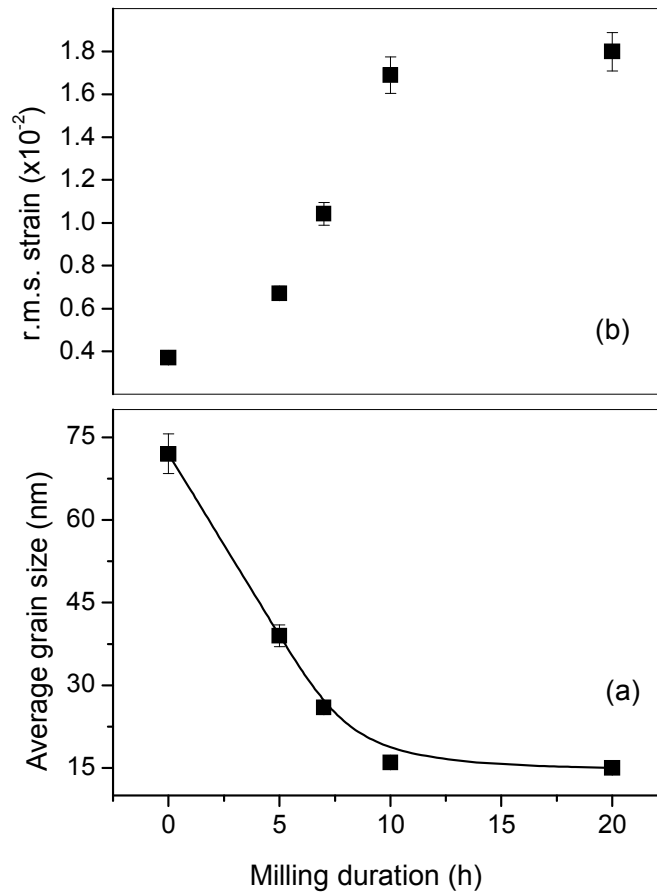
Fig. 5.2. The **(a)** average grain size and **(b)** r.m.s. strain for the Sm(Co,Fe,Cu,Zr)$_7$ compound milled for various durations.

distribution of strains, and θ is the angle of diffraction. The r.m.s. strain increases with milling up to 10 h and becomes almost constant on further milling up to 20 h as shown in Fig. 5.2.(b).

Figure 5.3 shows the SEM micrographs of the as-cast, 10 h milled and 20 h milled Sm(Co,Fe,Cu,Zr)$_7$ samples. The as-cast samples have micron-sized particles as seen from the SEM picture. On milling to 10 h, the particles become submicron in size around 0.6 – 0.9 μm and also some particles are found to be slightly agglomerated. The repeated breaking and welding of the particles leads to a change in the particle size and morphology. When milled for 20 h, the small particles are welded together to form agglomerates as visible from the SEM pictures.
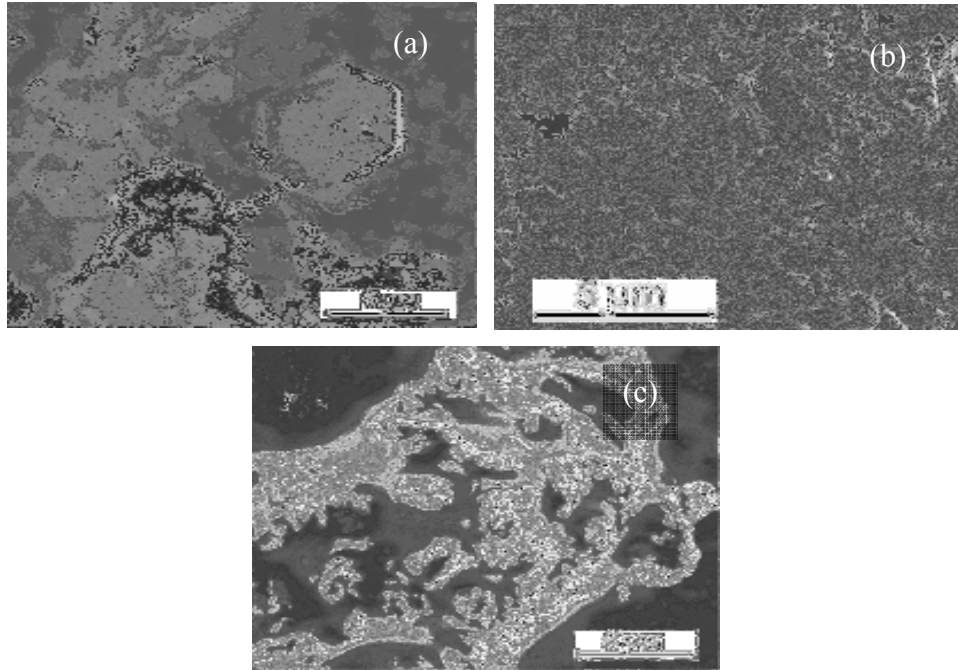
Fig. 5.3. The SEM pictures of the **(a)** as-cast, **(b)** 10 h milled and **(c)** 20 h milled Sm(Co,Fe,Cu,Zr)$_7$ compound.

5.3.2.   Magnetic properties

5.3.2.1. Coercivity vs. milling time

Figure 5.4.(a) and (b) show the hysteresis loops of the bulk and the 10 h milled Sm(Co,Fe,Cu,Zr)$_7$ samples respectively at 300 K. The coercivity of the samples increases on milling, whereas the saturation magnetization remains almost constant at 60 A m^2/kg. The smooth hysteresis loop is indicative of the presence of a single phase only; otherwise, the presence of two or more magnetic phases would result in a kink in the hysteresis loop in the absence of exchange coupling. Figure 5.5 shows the coercivity and remanence ratio for the Sm(Co,Fe,Cu,Zr)$_7$ powders for various milling times. The coercivity increases with milling from 44 kA/m for the as-cast to 280 kA/m for 10 h of milling and then decreases to 200 kA/m on further milling to 20 h. The coercivity for the SmCo$_{6.7}$Cu$_{0.3}$ alloy with the TbCu$_7$ structure was found to be 80 kA/m whereas it increased on annealing the ball-milled sample with the formation of Th$_2$Zn$_{17}$ structure [20]. The melt-spun ribbons of Sm(Co$_{0.85}$Fe$_{0.15}$)$_{7.6}$ with the TbCu$_7$ structure have shown a higher coercivity of 212 kA/m with grain size reduction to 5 – 0.5 μm [8] whereas for the SmCo$_{6.4}$Zr$_{0.4}$ melt-spun ribbon
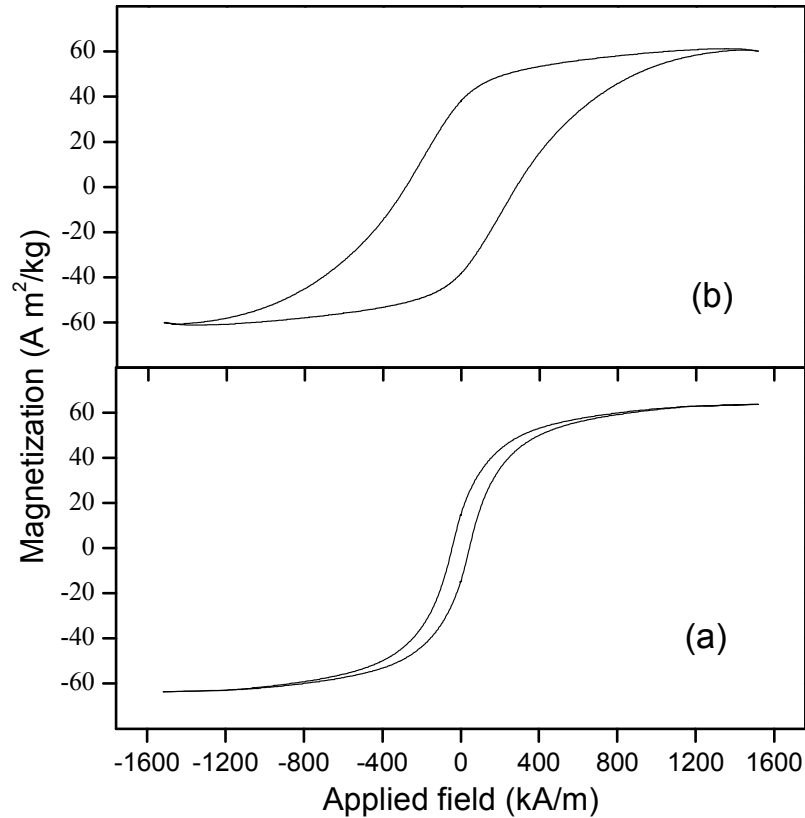
Fig. 5.4. The hysteresis loop at 300 K for the **(a)** as-cast and **(b)** 10 h milled Sm(Co,Fe,Cu,Zr)$_7$ compound.

with the same structure, the coercivity was only 144 kA/m, because of the texture effects [21]. Although the composition Sm(Co$_{0.85}$Fe$_{0.15}$)$_{7.6}$ is expected to show a lower coercivity due to the reduced anisotropy, because of the substitution of Fe, compared to SmCo$_{6.4}$Zr$_{0.4}$ with the same TbCu$_7$ structure the texture effect in the latter composition reduces the coercivity. Hence the estimation of grain size-dependent behaviour of coercivity in the melt-spun ribbons becomes difficult due to the texture effect. Chen *et al.* [22] showed an increase in the coercivity for the Sm$_2$Co$_{17}$ compound due to grain size reduction with a maximum value of 320 kA/m after milling for 20 min and a decrease with milling for higher duration due to the formation of amorphous phase. The increase of coercivity in the present study is believed to be due to the refinement in the grain size. The TbCu$_7$ structure remains stable with milling and the XRD pattern does not show any extra phases. This is supported by the magnetization measurement, which shows almost the same value for the magnetization even after milling. Thus the increase in coercivity with milling is due to the
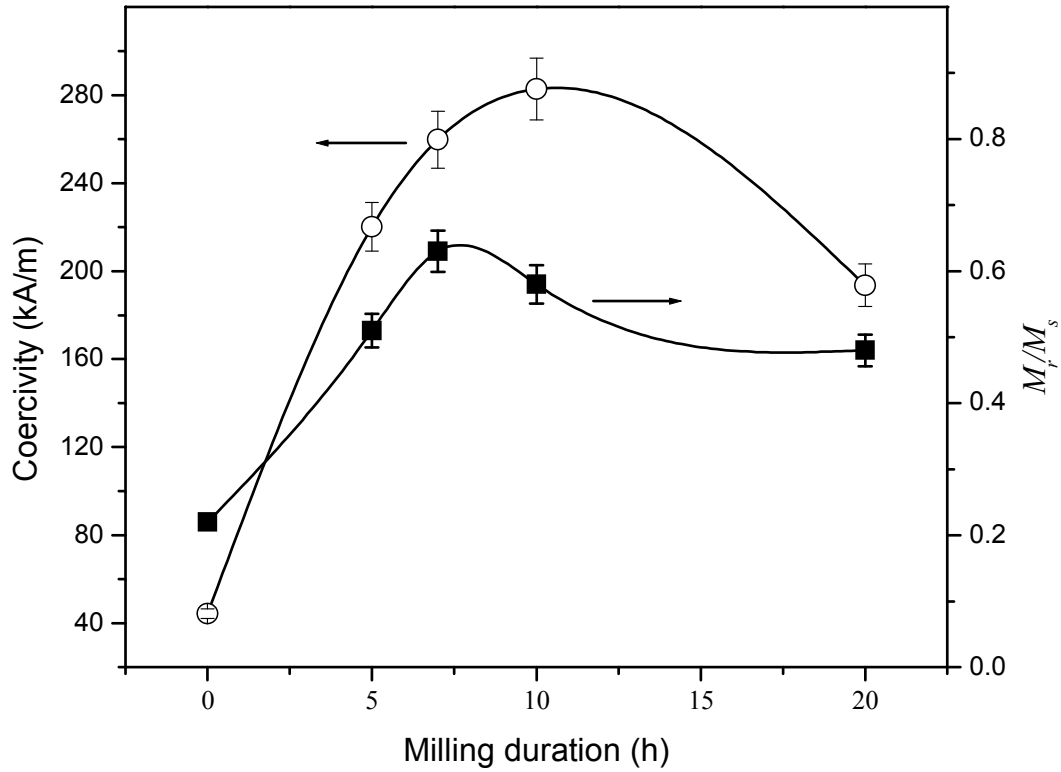
Fig. 5.5. The coercivity and remanence ratio of the Sm(Co,Fe,Cu,Zr)$_7$ compound milled for various durations. (The continuous lines are guide to the eye).

particle size reduction approaching the single domain state. The milling of the particles in the toluene medium, compared to the samples milled in an inert atmosphere, has facilitated the formation of less agglomerated particles on milling up to 10 h resulting in an increase in coercivity. The critical diameter D_c of the single domain particles can be estimated using the relation [23]

$$D_c = C_o \frac{\sqrt{AK_1}}{\mu_o M_s^2} \tag{5.1}$$

where C_o=72, A is the exchange constant which is of the order of 10 pJ/m [23], K_1 is the magnetic anisotropy constant, and M_s is the saturation magnetization. By substituting the values of K_1 calculated from the anisotropy field and M_s reported in the literature [24] for the SmCo$_{7-x}$Zr$_x$ compound with the TbCu$_7$ structure in Eq. (5.1), the critical size of the single domain is calculated to be 706 nm, assuming that the particles are spherical in shape. This value is subject to a small error that may arise due to a slight difference in the values

of *A* and K_1 of the two compositions. Since the high-energy ball milling would result in non-spherical shape for the particles, the actual critical size of the single domain particle should be larger as the elongated particles have a lower demagnetization factor [25]. Since the calculated single domain size is near the experimentally observed particle size of nearly 600 – 900 nm as seen from Fig. 5.3, the increase in the coercivity with milling up to 10 h is due to the particles approaching the single domain size. However, the decrease in coercivity for the 20 h milled samples is due to the agglomeration of the particles.

5.3.2.2. The δM measurements

According to the Stoner-Wohlfarth relation, non-interacting isolated particles have a remanence ratio below 0.5. But in the present study, the remanence ratio increases with milling and becomes greater than 0.5 after 5 h of milling which decreases again for the 20 h milled samples. The enhanced remanence ratio suggests the presence of exchange or dipolar interaction between the particles [26,27]. In order to verify the nature of interactions, δM studies were performed at 300 K for the milled samples. The δM values are calculated from the Isothermal Remanence Magnetization (IRM) measurements, which is done by plotting the remanent magnetization as a function of field from a demagnetized sample and from the Direct Current Demagnetization (DCD) measurements by applying a reverse field and measuring the demagnetization curve of the sample. From these measurements the parameter δM, which is defined as [28]

$$\delta M = \frac{\left\{ M_D(H) - \left[M_r(H_{max}) - 2M_R(H) \right] \right\}}{M_r(H_{max})} \tag{5.2}$$

where $M_D(H)$ is the DCD remanence, $M_R(H)$ is the IRM, and $M_r(H_{max})$ is the saturation remanence, is plotted against the applied field H. A positive value for δM represents exchange interaction and a negative value represents dipolar interaction between the grains whereas a zero value is obtained for non-interacting particles with uniform pinning of domain walls [29].

Figure 5.6 shows the variation of δM at 300 K with applied magnetic field for various milling durations for Sm(Co,Fe,Cu,Zr)$_7$. The nonzero value for δM suggests that there is no uniform pinning of domain walls and the negative value for all the samples confirms the presence of dipolar interactions. The dipolar coupling decreases with particle
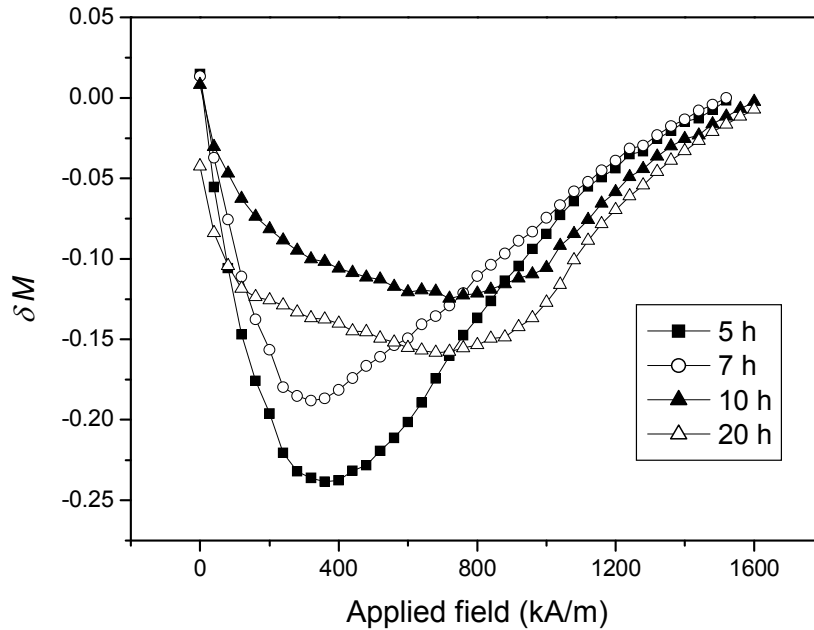
Fig. 5.6. The δM curves at 300 K for the Sm(Co,Fe,Cu,Zr)$_7$ compound milled for various durations. (The continuous curves are guide to the eye).

size reduction on milling from 5 h to 10 h as could be seen from the decrease in the peak height. However, the area of the δM peak increases for the 10 h milled sample. The nonuniformity of particle sizes, which is inherent in the milled samples, results in a large distribution in dipolar interactions [30] for the 10 h milled samples. But, the dipolar interaction strength is observed to increase on further milling to 20 h, probably due to the stray fields [31,32] originating from defects and non-ideal grain boundaries introduced by milling. The dipolar interaction strength also depends on the positional disorder present in the system [33]. The observed decrease in the remanence ratio to less than 0.5 for the 20 h milled sample is likely to be due to the microstructural changes.

5.3.3. The temperature stability of the TbCu$_7$ structure

Figure 5.7 shows the thermomagnetization measurement, using TGA, of the as-cast Sm(Co,Fe,Cu,Zr)$_7$ compound up to 923 K. The as-cast alloy shows an increase in the weight above 743 K denoted by T_{cr} as shown in the TGA curve (Fig. 5.7) which may be
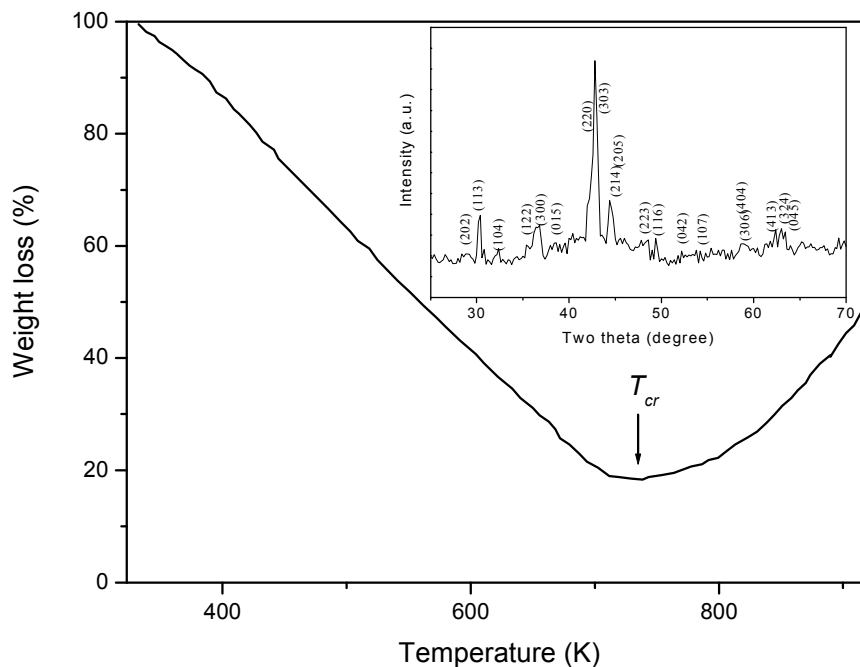
Fig. 5.7. The thermomagnetic measurement using TGA for the as-cast $Sm(Co,Fe,Cu,Zr)_7$ compound. Inset shows the XRD of the as-cast $Sm(Co,Fe,Cu,Zr)_7$ compound annealed at 873 K with the Th_2Zn_{17} structure.

due to the crystallization of another phase. The XRD, shown in the inset of Fig. 5.7, reveals that the crystallized phase is the ordered Th_2Zn_{17} structure which is responsible for the observed increase in the weight in the thermomagnetization measurement beyond 743 K due to the higher value of its magnetization than that of the $TbCu_7$ structure.

5.3.4. Mössbauer studies

Mössbauer spectroscopy is effectively used in studying the site preference of the substituting elements in rare earth permanent magnetic materials [34-37]. Figure 5.8 shows the ^{57}Fe Mössbauer spectrum at 300 K of the 10 h milled $Sm(Co,Fe,Cu,Zr)_7$ compound with the corresponding Mössbauer parameters presented in Table 5.1. The ratio of the intensities of the peaks in a sextet was fixed as 3:2:1:1:2:3 assuming random orientation of grains in polycrystalline samples. The Mössbauer spectrum was fitted with four sextets corresponding to the 2e, 6l, 3g, and 2c sites of the disordered $TbCu_7$ structure and a singlet of unknown origin.
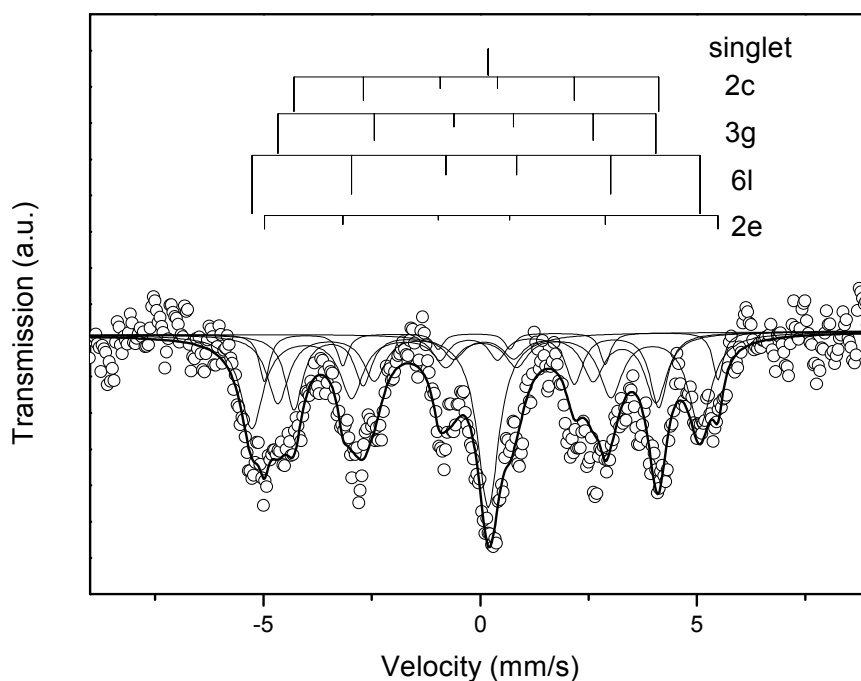
Fig. 5.8. The Mössbauer spectrum at 300 K of the 10 h milled Sm(Co,Fe,Cu,Zr)$_7$ compound.

Table 5.1. The Mössbauer parameters at 300 K of the 10 h milled Sm(Co,Fe,Cu,Zr)$_7$ compound.

Hyperfine field ($\pm$ 0.1 T)	Isomer shift* ($\pm$ 0.05 mm/s)	Quadrupole splitting ($\pm$ 0.06 mm/s)	Linewidth ($\pm$ 0.05 mm/s)	Relative Intensity ($\pm$ 1 %)	sites
32.4	0.17	0.40	0.29	7.7	2e
32.0	0.08	0.13	0.64	33.8	6l
27.0	0.01	0.39	0.60	23.2	3g
26.1	-0.06	-0.18	0.48	20.3	2c
0.0	0.00	0.00	0.61	15.0	unknown

* relative to α-Fe at 300 K.

A similar study has been reported by Bessais and Djéga-Mariadassou for their SmFeCoTi alloys [37]. The hyperfine fields of the sextets were observed to be $H_{hf}(2e) > H_{hf}(6l) > H_{hf}(3g) > H_{hf}(2c)$ according to the Fe- coordination number. The lowest hyperfine

field for the 2c site and the highest one for the dumbbell 2e site are due to the smallest and the highest coordination of Fe respectively at the two sites in accordance with the structural details reported in literature [38]. The isomer shift has been assigned as $\delta(2e) > \delta(6l) > \delta(3g) > \delta(2c)$ in accordance with the Wigner-Seitz cell (WSC) volume [37]. The hyperfine field of 32.4 T arises from the Fe in the 2e dumbbell site which has the highest number of nearest neighbour iron atoms. The relative intensity of the 2e sextet is also the smallest among the four sextets since this site is formed by the replacement of a Sm atom randomly by a dumbbell Fe pair. The high values of the quadrupole splitting for the 2e and 3g sites suggest that the Fe environment at these sites is highly asymmetric. The Mössbauer spectrum of the 6l site has the highest relative intensity as this site has the largest Fe occupancy. The Mössbauer spectra of the other two sites 3g and 2c have almost equal relative intensities. Although the relative abundance of 2c site is the lowest and equal only to the 2e site, the relatively large intensity of the Mössbauer sextet arising from the 2c site indicates that Fe preferentially occupies the 2c site. A singlet with a relative intensity of 15 % could not be correlated to any phase or to any site. The presence of the singlet has already been observed in the Mössbauer spectrum of the Sm-Co alloys but it is not attributed to any site or phase [39]. Mössbauer results thus confirm that the hyperfine field and isomer shift values of the four sites are in the order of (2e) > (6l) > (3g) > (2c) according to the structural details of the $TbCu_7$ structure.

5.4. Conclusion

The coercivity of the $Sm(Co,Fe,Cu,Zr)_7$ compound was varied from 44 kA/m for the bulk to 280 kA/m by controlling the grain size using high-energy ball milling without affecting the saturation magnetization. Interestingly, a high coercivity could be obtained in mechanically milled powders without subjecting them to any post annealing treatment. The increase in the coercivity is attributed to the particles approaching single domain size. The particles showed dipolar coupling whose strength is found to decrease with milling up to 10 h. The Mössbauer spectrum of the $Sm(Co,Fe,Cu,Zr)_7$ alloy with the $TbCu_7$ structure suggests that Fe preferentially occupies the 2c site.

References

[1]   J. F. Liu, T. Chui, D. Dimitrov, and G. C. Hadjipanayis, Appl. Phys. Lett. **76** (1998) 3007.

[2]   K. H. J. Buschow, in *Handbook of Magnetic Materials* (Elsevier, Amsterdam, 1997) Vol. 10.

[3]   K. Kumar, J. Appl. Phys. **63** (1988) R13.

[4]   I. A. Al-Omari, J. Zhou, and D. J. Sellmyer, J. Alloys and Compds. **298** (2000) 295.

[5]   M. Q. Huang, M. Drennan, W. E. Wallace, M. E. McHenry, Q. Chen, and B. M. Ma, J. Appl. Phys. **85** (1999) 5663 .

[6]   P. A. I. Smith, J. Ding, R. Street, and P. G. McCormick, Scripta Mater. **34** (1996) 61.

[7]   A. Yan, A. Bollero, K. -H. Müller, and O. Gutfleisch, Appl. Phys. Lett. **80** (2002) 1243.

[8]   C. H. Chen, S. Kodat, M. H. Walmer, S-F Cheng, M. A. Willard, and V. G. Harris, J. Appl. Phys. **93** (2003) 7966.

[9]   V. G. Harris, M. Liou, B. N. Das, V. M. Browning, J. E. Snyder, M. Rubinstein, S. H. Lawrence, R. Littleton III, and D. P. Pappas, J. Appl. Phys. **81** (1997) 5121.

[10] J. E. Shield and B. E. Meacham, J. Appl. Phys. **87** (2000) 2055.

[11] J. Zhou, R. Skomski, C. Chen, G. C. Hadjipanayis, and D. J. Sellmyer, Appl. Phys. Lett. **77** (2000) 1514.

[12] J. X. Zhang, L. Bessais, C. Djéga-Mariadassou, E. Leory A. Percheron-Guégan, and Y. Champion, Appl. Phys. Lett. **80** (2002) 1960 .

[13] D. L. Leslie-Pelecky and R. L. Schalek, Phys. Rev. B **59** (1999) 457.

[14] J. Sort, S. Suriñach, J. S. Muñoz, M. D. Baró, J. Nogués, G. Chouteau, V. Skumryev, and G. C. Hadjipanayis, Phys. Rev. B **65** (2002) 174420.

[15] J. Sort, J. Nogués, S. Suriñach, J. S. Muñoz, M. D. Baró, E. Chappel, F. Dupont, and G. Chouteau, Appl. Phys. Lett. **79** (2001) 1142.

[16] G. C. Hadjipanayis, J. Appl. Phys. **55** (1984) 2091.

[17] K. H. J. Buschow and A. S. Van der Goot, Acta Cryst. B **27** (1971) 1085.

[18] F. J. Cadieu, H. Hegde, N. Kamprath, A. Navarathna, and R. Rani, Proc. 11th Int. Workshop on Rare Earth Magnets and their Applications, Pennsylvania, Vol. II (1990) p.463.

[19] J. Friedel, *Dislocations* (Pergamon, Oxford, 1964).

[20] M. Venkatesan, C. Jiang, and J. M. D. Coey, J. Magn. Magn. Mater. **242-245** (2002) 1350 .

[21] A. R. Yan, Z. G. Sun. W. Y. Zhang, H. W. Zhang, and B. G. Shen, Appl. Phys. A **71** (2000) 311.

[22] Z. Chen, X. Meng-Buray, H. Okumura, and G. C. Hadjipanayis, J. Appl. Phys. **87** (2000) 3409.

[23] R. Skomski, J. Phys.:Condens. Mater. **15** (2003) R841.

[24] M. Q. Huang, W. E. Wallace, M. McHenry, Q. Chen, and B. M. Ma, J. Appl. Phys. **83** (1998) 6718.

[25] B. D. Cullity, *Introduction to Magnetic Materials* (Addison-Wesley, Masachusetts, 1972).

[26] Q. Chen, B. M. Ma, B. Lu, Q. Huan, and D. E. Laughlin, J. Appl. Phys. **85** (1999) 5917.

[27] H. Ku and J. Y. Li, Phys. Rev. B **68** (2003) 212402.

[28] P. E. Kelly, K. O'Grady, P. I. Mayo, and R. W. Chantrell, IEEE Trans. Magn. **25** (1989) 3881.

[29] G. C. Hadjipanayis and A. Kim, J. Appl. Phys. **63** (1988) 3310.

[30] J. Sort, S. Suriñach, J. S. Muñoz, M. D. Baró, J. Nogués, S. de Brion, and G. Chouteau, J. Appl. Phys. **93** (2003) 8140.

[31] R. Fisher and H. Kronmüller, J. Appl. Phys. **83** (1998) 3271.

[32] V. Neu, A . Hubert, and L. Schultz, J. Magn. Magn. Mater. **189** (1998) 391.

[33] M. Porto, J. Appl. Phys. **92** (2002) 6057.

[34] M. Manivel Raja and A. Narayanasamy, J. Appl. Phys. **84** (1998) 5715.

[35] M. Manivel Raja and A. Narayanasamy, J. Magn. Magn. Mater. **159** (1996) 345.

[36] L. C. C. M. Nagamine, H. R. Rechenberg, and A. E. Ray, J. Magn. Magn. Mater. **89** (1990) L270.

[37] L. Bessais and C. Djéga-Mariadassou, Phys. Rev. B **63** (2001) 54412.

[38] M. Forker, A. Julius, M. Schulte, and D. Best, Phys. Rev. B **57** (1998) 11565.

[39] Z. W. Liu, X. Z. Zhou, and A. H. Morrish, Phys. Rev. B **51** (1995) 2891.